The EMBO Journal (2013) 32, 2764–2778
www.embojournal.org

SOURCE DATA | TRANSPARENT PROCESS

THE EMBO JOURNAL

Antagonistic functions between the RNA chaperone Hfq and an sRNA regulate sensitivity to the antibiotic colicin

Hubert Salvail[1], Marie-Pier Caron, Justine Bélanger and Eric Massé*

Department of Biochemistry, RNA Group, University of Sherbrooke, Sherbrooke, Quebec, Canada

The RNA chaperone Hfq is a key regulator of the function of small RNAs (sRNAs). Hfq has been shown to facilitate sRNAs binding to target mRNAs and to directly regulate translation through the action of sRNAs. Here, we present evidence that Hfq acts as the repressor of *cirA* mRNA translation in the absence of sRNA. Hfq binding to *cirA* prevents translation initiation, which correlates with *cirA* mRNA instability. In contrast, RyhB pairing to *cirA* mRNA promotes changes in RNA structure that displace Hfq, thereby allowing efficient translation as well as mRNA stabilization. Because CirA is a receptor for the antibiotic colicin Ia, in addition to acting as an Fur (Ferric Uptake Regulator)-regulated siderophore transporter, translational activation of *cirA* mRNA by RyhB promotes colicin sensitivity under conditions of iron starvation. Altogether, these results indicate that Fur and RyhB modulate an unexpected feed-forward loop mechanism related to iron physiology and colicin sensitivity.

The EMBO Journal (2013) **32,** 2764–2778. doi:10.1038/emboj.2013.205; Published online 24 September 2013
Subject Categories: RNA; proteins; microbiology & pathogens
Keywords: *cirA*; colicin; Hfq; sRNA; translation activation

Introduction

To successfully occupy their specific niche, bacteria have developed strategies to prevent growth of competitors. One of these strategies is the production of bacteriocins that are protein toxins produced by most bacteria to compete with similar or closely related strains (Riley and Wertz, 2002). Colicins are *E. coli*-specific bacteriocins released in the environment to kill other *E. coli* strains. They have been shown to play key roles in promoting diversity and coexistence of bacterial populations in the mammalian colon (Kerr *et al*, 2002; Kirkup and Riley, 2004). Colicins are divided into two subgroups according to the energy-transducing system they use to invade targeted cells. Whereas group A colicins use the Tol system, group B colicins use the Ton system (Lazdunski *et al*, 1998; Braun *et al*, 2002). Colicins exert their activity through a variety of mechanisms ranging from pore formation in the inner membrane to nuclease activity against DNA or RNA (Kleanthous, 2010).

Colicin gene clusters are generally carried on a plasmid and typically encode an immunity protein, which is expressed constitutively to protect the cell from its own colicin attack. The cluster also encodes a lysis protein that allows the release of the colicin in the environment through cell lysis (Riley, 1993a, 1993b). Once released, colicins bind with high affinity to outer membrane receptors of the target cells. Proteins recognized by colicins range from vitamin transporter to siderophore receptors (e.g., CirA, FepA, and FhuA).

One of the most extensively studied pore-forming colicin is colicin Ia, which targets the outer membrane protein (OMP) CirA (Buchanan *et al*, 2007; Jakes and Finkelstein, 2010). Colicin Ia is a 69-kDa protein that inserts into the inner membrane of the target cell to form a channel responsible for cell death (Wiener *et al*, 1997). CirA is a TonB-dependent transporter involved in the uptake of ferric iron (Fe^{3+}) complexed with catechol siderophores such as dihydroxybenzoate (DHB) and dihydroxybenzoyl serine (DHBS), which are respectively precursor and breakdown product of the siderophore enterobactin (Hantke, 1990). As for most genes involved in iron uptake, *cirA* transcription is repressed by the Fur (Ferric Uptake Regulator) protein bound to ferrous iron (Fe^{2+}) (Griggs *et al*, 1987). Moreover, two redundant small RNAs (sRNAs), OmrA and OmrB, have also been shown to repress *cirA* translation under conditions of high osmolarity (Guillier and Gottesman, 2006, 2008).

Bacterial sRNAs are key regulators of cellular functions by modulating gene expression in response to various environmental cues (Gottesman and Storz, 2010). These sRNAs regulate target mRNAs by direct base pairing to positively or negatively affect their translation and stability (Storz *et al*, 2011). In most cases, sRNAs require the RNA chaperone Hfq for optimal regulation by promoting sRNA-mRNA pairing and by stabilizing some sRNAs *in vivo* (Vogel and Luisi, 2011; Andrade *et al*, 2012). Hfq can also act as a translational repressor by competing directly with initiating 30S ribosomal subunit for accessibility to the ribosome binding site (RBS) (Vytvytska *et al*, 2000; Desnoyers and Massé, 2012).

The sRNA RyhB, which regulates iron homeostasis, is one of the most studied Hfq-dependent sRNAs. Under iron-rich conditions, Fe^{2+}-Fur represses *ryhB* transcription. In contrast, during iron starvation conditions, Fur becomes inactive and relieves repression of *ryhB* (Massé and Gottesman, 2002; Salvail and Massé, 2011). Under these conditions, RyhB directly regulates ~20 different mRNAs encoding iron-using

*Corresponding author. Department of Biochemistry, RNA Group, Faculty of Medicine and Health Sciences, University of Sherbrooke, 3201 Jean Mignault Street, Sherbrooke, Quebec, Canada J1E 4K8. Tel.: +1 819 821 8000 ext. 75475; E-mail: eric.masse@usherbrooke.ca
[1]Present address: Section of Microbial Pathogenesis, Boyer Center for Molecular Medicine, Howard Hughes Medical Institute, Yale School of Medicine, 295 Congress Avenue, New Haven, CT 06536-0812, USA.

Received: 22 January 2013; accepted: 14 August 2013; published online: 24 September 2013

proteins. By binding to those mRNAs, RyhB shuts down translation and stimulates their rapid degradation through the action of RNase E (Massé *et al*, 2003; Massé *et al*, 2005). RyhB also promotes siderophore production through repression of *cysE* mRNA that encodes a serine acetyltransferase, which results in an increased flux of serine into enterobactin production (Salvail *et al*, 2010).

In addition, RyhB can act as a gene activator. Indeed, RyhB activates translation of the Fur-independent *shiA* mRNA that encodes a transporter of shikimate, an intermediate in the synthesis of enterobactin (Prévost *et al*, 2007). Hfq binds the 5′-untranslated region (UTR) of *shiA* and potentially promotes the formation of an inhibitory structure that sequesters the translation initiation region (TIR) and limits translation. However, under conditions of iron starvation, RyhB base pairs with *shiA* mRNA to disrupt the inhibitory structure, thereby favouring translation and transcript stabilization. This mechanism is reminiscent of similar cases of translational activation by sRNAs such as activation of *rpoS* by DsrA (Sledjeski *et al*, 1996; McCullen *et al*, 2010) and activation of *glmS* mRNA by GlmZ sRNA (Urban and Vogel, 2008).

In this work, we present evidence that RyhB is a novel regulator of *cirA* expression. We showed that RyhB expression was essential for CirA synthesis during iron starvation. Our data further suggested that in the absence of RyhB, Hfq repressed *cirA* mRNA translation, thereby causing rapid transcript turnover through the action of RNase E and low accumulation of CirA. RyhB pairing to *cirA* mRNA activated its translation and prevented its destabilization by RNase E. The resulting increased levels of CirA transporter made the cells sensitive to the bactericidal action of colicin Ia. This new RyhB-mediated regulation was unexpected considering that *cirA* is, to our knowledge, the first Fur-regulated gene to require post-transcriptional activation by RyhB to be expressed during iron starvation. The Fur-RyhB-*cirA* regulatory circuit forms a coherent feed-forward loop (Fur represses *cirA* and *ryhB* while RyhB activates *cirA*), predicted to confer altered regulatory dynamics in comparison to direct regulation by Fur (Mangan and Alon, 2003; Beisel and Storz, 2010). In addition to its role as a gene silencer, our results confirmed the role of RyhB in gene activation.

Results

RyhB expression is essential for CirA production

Previous microarray results have shown that RyhB expression resulted in a 3.3-fold increase in *cirA* transcript levels in a Δ*fur* Δ*ryhB* background (Massé *et al*, 2005). To extend these results, we used quantitative real-time PCR (qRT–PCR) to monitor *cirA* mRNA levels after a 20-min expression of RyhB in Δ*ryhB* and Δ*fur* Δ*ryhB* backgrounds, as in the case of the microarray study. Results showed that *cirA* transcript levels increased 4.7-fold upon RyhB expression in the Δ*fur* Δ*ryhB* background (Figure 1A). This increase was higher than the previously characterized RyhB-positive target *shiA* (2.3-fold increase) (Prévost *et al*, 2007). Intriguingly, RyhB expression in a Δ*ryhB* background resulted in a 3.3-fold decrease in *cirA* transcript levels. We have previously reported that RyhB expression under these conditions promoted an increase in free intracellular iron concentration (Jacques *et al*, 2006). Thus, the decrease in *cirA* mRNA levels observed here may result from Fe^{2+}-Fur repression, as observed in the case of Fur-regulated genes (Massé *et al*, 2005). In contrast, RyhB still upregulated the expression of the Fur-independent *shiA* gene in the Δ*ryhB* background (Figure 1A).

Full-length *cirA* mRNA expression was monitored by northern blot following pulse expression of RyhB in the Δ*fur* Δ*ryhB* background. This showed that *cirA* transcript accumulation following RyhB expression was swift with maximal transcript accumulation following 8 min of sRNA induction (Figure 1B, lane 5). However, despite high *cirA* promoter activity in the Δ*fur* Δ*ryhB* background (Supplementary Figure S1A, see pNM12), *cirA* transcript poorly accumulated in the absence of RyhB (Figure 1B, lanes 8–14). Moreover, RyhB had no significant effect on *cirA* promoter (Supplementary Figure S1A, pNM12 and pBAD-*ryhB*), suggesting that RyhB regulated *cirA* post-transcriptionally.

Since RyhB is naturally expressed during iron starvation, we next studied the endogeneous effect of RyhB on *cirA* expression in iron-free minimal medium. Results showed that *cirA* mRNA levels in WT cells correlated with RyhB levels (Figure 1C, lanes 1 and 2). In contrast, Δ*ryhB* cells did not accumulate *cirA* transcripts at any time (Figure 1C, lanes 3 and 4), despite promoter activity similar to WT cells (Supplementary Figure S1B, WT and Δ*ryhB*). Inactivation of *fur* resulted in increased levels of *cirA* mRNA as compared to WT cells (Figure 1C, lanes 1 and 2, and lanes 5 and 6). This behaviour probably resulted from increased *cirA* promoter activity (Supplementary Figure S1B, WT and Δ*fur*) due to the absence of Fe^{2+}-Fur repression. The absence of Fur repression also resulted in higher levels of RyhB in Δ*fur* cells as compared to WT cells (Figure 1C, lanes 1 and 2, and lanes 5 and 6) which may also contribute to increased levels of *cirA* mRNA. Strikingly, inactivation of *ryhB* in a Δ*fur* background resulted in a severe decrease in *cirA* transcript levels (Figure 1C, compare lanes 5 and 6 with lanes 7 and 8), despite an increase in *cirA* promoter activity (Supplementary Figure S1B, Δ*fur* and Δ*fur* Δ*ryhB*, OD_{600} of 0.6). Taken together, these results suggested that RyhB expression was essential to promote *cirA* transcript accumulation upon iron starvation.

Because our data indicated that RyhB was essential for *cirA* expression, we hypothesized that RyhB could stabilize *cirA* mRNA. To address this, we determined the half-life of *cirA* mRNA under conditions where RyhB was expressed (pBAD-*ryhB*) or not (pNM12). Because full-length *cirA* accumulated poorly in the Δ*fur* Δ*ryhB* background in LB medium (Figure 1B), we performed a primer extension using a reverse primer complementary to the beginning of *cirA* coding sequence. This approach was found to be sensitive enough to observe *cirA* mRNA expression in the absence of RyhB (Figure 1D, lane 2). While significant amounts of *cirA* transcripts were detected after 8 min in the presence of RyhB (Figure 1D, lane 12), most of the *cirA* mRNA disappeared after 2 min in the absence of RyhB (Figure 1D, lane 3). Densitometry analysis revealed that *cirA* mRNA had a half-life of 5 min when RyhB was expressed (pBAD-*ryhB*) but of less than 2 min in the absence of RyhB (Figure 1D).

Since RyhB promoted *cirA* mRNA accumulation, we next sought to determine the effect on CirA protein expression. Because CirA is an OMP, we compared the OMP profiles of Δ*fur*, Δ*fur* Δ*cirA*, Δ*fur* Δ*ryhB*, and Δ*fur* Δ*ryhB* Δ*hfq* cells

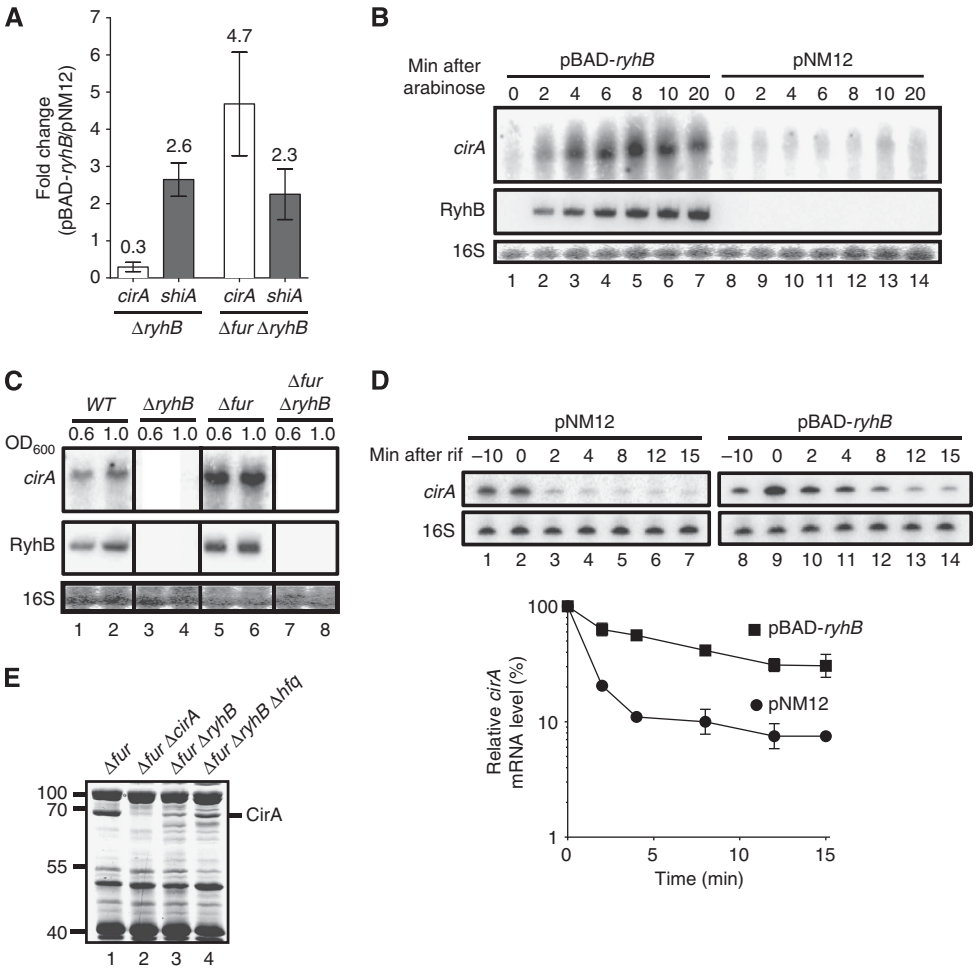

Figure 1 RyhB expression is essential for CirA production. (**A**) Quantitative RT-PCR (qRT-PCR) analysis of RyhB effect on *cirA* and *shiA* mRNA levels. Strains EM1455 (Δ*ryhB*) and EM1493 (Δ*fur* Δ*ryhB*), each carrying either pBAD-*ryhB* or control plasmid pNM12, were grown in LB medium. Arabinose was added (0.1%, total concentration) to an OD_{600} of 0.5, followed by total RNA extracted after 20 min. Primers complementary to *cirA* and *shiA* open reading frames (ORFs) were used for qRT–PCR assays. Mean and standard deviation (s.d.) values of triplicate samples are shown. (**B**) Northern blot analysis of RyhB effect on *cirA* mRNA levels. Strain EM1493 (Δ*fur* Δ*ryhB*) carrying pBAD-*ryhB* or control plasmid pNM12 was grown in LB medium. Arabinose was added (0.1%, total concentration) to an OD_{600} of 0.5 and total RNA was extracted at the indicated time points. A probe complementary to *cirA* ORF was used. (**C**) Northern blot analysis of RyhB and Fur effects on *cirA* mRNA levels in cells grown under iron-poor conditions. Strains EM1055 (WT), EM1238 (Δ*ryhB*), KP392 (Δ*fur*) and KP393 (Δ*fur* Δ*ryhB*) were grown in M63 iron-free glucose minimal medium and total RNA was extracted at the indicated values of OD_{600}. A probe complementary to *cirA* ORF was used. (**D**) Primer extension analysis of RyhB effect on *cirA* mRNA stability. Strain EM1493 (Δ*fur* Δ*ryhB*) carrying pBAD-*ryhB* or control plasmid pNM12 was grown in LB medium and arabinose was added (0.1%, total concentration) to an OD_{600} of 0.5 (−10 time point). Rifampicin (250 μg/ml, final concentration) was added 10 min after the addition of arabinose (0 time point) and total RNA was extracted at the indicated time points. Primers complementary to *cirA* (EM1408) and 16S rRNA (EM345) were used to perform primer extension reactions on total RNA samples. Primer extension signals of two independent experiments were quantified by densitometry and normalized to time zero (0) for both pNM12 and pBAD-*ryhB*. Mean and s.d. values of duplicate experiments are shown. (**E**) Coomassie-stained SDS gel of outer membrane proteins (OMPs) extracts from KP392 (Δ*fur*), HS437 (Δ*fur* Δ*cirA*), KP393 (Δ*fur* Δ*ryhB*) and MPC253 (Δ*fur* Δ*ryhB* Δ*hfq*) cells grown in LB medium at an OD_{600} of 1.0. Molecular sizes of co-migrating proteins (L) are indicated at the left in kDa. Source data for this figure is available on the online supplementary information page.

grown in LB media. Comparison of the profiles between Δ*fur* and Δ*fur* Δ*ryhB* cells revealed the presence of a protein of ~65 kDa for which the levels of expression were very low in Δ*fur* Δ*ryhB* cells as compared to Δ*fur* cells (Figure 1E, lanes 1 and 3). Intriguingly, the absence of Hfq in Δ*fur* Δ*ryhB* Δ*hfq* cells appears to improve the expression of the 65-kDa protein as compared to Δ*fur* Δ*ryhB* cells (Figure 1E, compare lanes 3 and 4). Because this protein was absent in Δ*fur* Δ*cirA* cells (Figure 1E, lane 2) and since the estimated molecular weight of CirA is between 54 and 74 kDa (Buchanan *et al*, 2007), we assumed this protein to be CirA. The bulk of these results suggested that RyhB was essential for CirA production.

RyhB directly activates cirA in vivo

Data reported above (Figure 1) suggested that RyhB activated *cirA* through direct pairing with its mRNA. Bioinformatic analysis using the TargetRNA software (Tjaden *et al*, 2006) suggested potential pairing of RyhB with *cirA* 5′-UTR in the region −58 to −41 relative to the AUG start codon (Figures 2 and 3A). We then proceeded to investigate this potential RyhB pairing site by chemical *in vitro* analysis. A 5′-end-labelled *cirA* transcript containing the whole 5′-UTR and 79 additional nucleotides (nt) from the coding region was incubated in the presence or absence of a 20-fold molar excess of unlabelled RyhB, followed by a partial digestion by lead acetate (PbAc, cleaves unpaired residues). Results

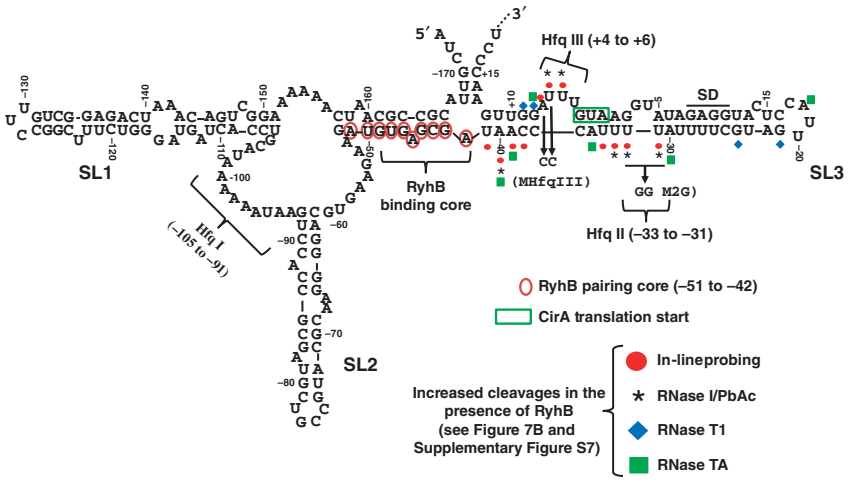

Figure 2 The 5′-UTR of *cirA* mRNA potentially forms an inhibitory structure preventing translation initiation. RNA-fold prediction of *cirA* 5′-UTR secondary structure (nucleotides −173 to +18 relative to the AUG start codon). The RyhB pairing core, the Hfq binding sites, the M2G mutation of Hfq binding site II and the MHfqIII mutation of Hfq binding site III are indicated. Probing results presented in Figure 7B and Supplementary Figure S7 are summarized here. Stem-loop structures are numbered (SL1, SL2, and SL3).

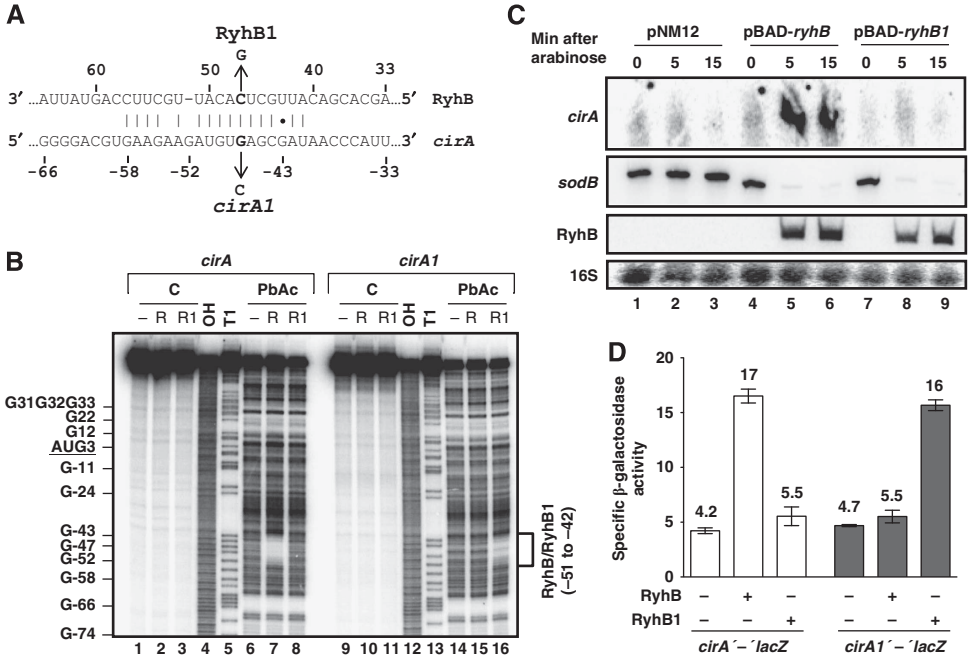

Figure 3 RyhB base pairs with *cirA* mRNA *in vivo*. (**A**) TargetRNA prediction of pairing between RyhB and *cirA* mRNA. The *cirA1* and RyhB1 mutations used in (**B**–**D**) are indicated. (**B**) Lead acetate (PbAc) probing of RyhB pairing with *cirA* mRNA. 5′-end-labelled *cirA* or *cirA1* mRNAs (nucleotides −173 to +78 relative to the AUG start codon) were incubated in the absence or in the presence of RyhB (R) or RyhB1 (R1) before addition of PbAc. C, non-reacted controls; OH, alkaline ladder; T1, RNase T1 ladder (guanine residues). (**C**) Northern blot analysis of arabinose-induced RyhB1 effect on *cirA* mRNA levels. Strain EM1493 (Δ*fur* Δ*ryhB*) carrying pBAD-*ryhB*, pBAD-*ryhB1* or control plasmid pNM12 was grown in LB medium. Arabinose (0.1%, total concentration) was added to an OD_{600} of 0.5 and total RNA was extracted at the indicated time points. Probes complementary to *cirA* and *sodB* open reading frames (ORFs) were used. (**D**) Effect of arabinose-induced RyhB and RyhB1 on *cirA*′-′*lacZ* and *cirA1*′-′*lacZ* translational fusions in a Δ*fur* Δ*ryhB* background. Cells were grown in LB medium and arabinose (0.1%, total concentration) was added to an OD_{600} of 0.1. Specific β-galactosidase activity from three independent cultures was then measured 3 h later. Mean and standard deviation (s.d.) values are shown. Empty vector pNM12 was used as a control. Source data for this figure is available on the online supplementary information page.

showed that the addition of RyhB (R) protected from cleavage (Figure 3B, lanes 6 and 7) in the region −42 to −51 that corresponded to the predicted RyhB pairing core (Figures 2 and 3A).

To further confirm that RyhB paired directly with *cirA* mRNA *in vivo*, we constructed the RyhB1 allele in which nucleotide C47 was exchanged for G47 to decrease the strength of pairing with *cirA* (see details in Figure 3A). The cleavage assay showed that the addition of RyhB1 (R1) did not protect bases that were determined to be part of the RyhB pairing core (Figure 3B, lanes 6 and 8). These data strongly suggest that RyhB1 was not able to base pair with *cirA* mRNA *in vitro*. RyhB1 was then expressed using an arabinose-inducible vector and its effect on *cirA* mRNA levels was monitored by northern blot analysis. Results showed that in spite of similar levels of accumulation compared to RyhB (Figure 3C, lanes 5 and 6, and lanes 8 and 9), RyhB1 failed to promote *cirA* expression within 15 min as opposed to RyhB

expression that resulted in rapid accumulation of *cirA* transcripts (Figure 3C, lanes 4–6, and lanes 7–9). However, RyhB1 was still able to repress *sodB*, an RyhB-repressed gene (Figure 3C, lanes 7–9). This observation suggested that RyhB1 remained functional and that the loss of *cirA* regulation probably reflected a disruption of target-specific base pairing.

To further characterize RyhB-*cirA* interaction, we constructed the *cirA1* allele in which nucleotide G47 was changed to C47 to restore base pairing with RyhB1 (see Figure 3A for details). Results indicated that RyhB addition did not promote cleavage protection of *cirA1* (Figure 3B, lanes 14 and 15), indicating that RyhB was not able to base pair with *cirA1* mRNA. As predicted, the compensatory mutation introduced in RyhB1 was able to restore base pairing with *cirA1* since the nucleotides of *cirA1* that are part of the RyhB pairing core were protected from cleavage (Figure 3B, lane 14 and lane 16). We next performed *in vivo* covariation mutagenesis using *cirA′-′lacZ* and *cirA1′-′lacZ* translational fusions, harbouring region −280 to +33 with respect to the initiation codon. Results indicated that RyhB expression resulted in a four-fold activation of the *cirA′-′lacZ* translational construct but failed to activate *cirA1′-′lacZ* fusion while RyhB1 only activated the complementary *cirA1′-′lacZ* construct without affecting the *cirA′-′lacZ* construct (Figure 3D). Taken together, these data confirmed that RyhB promoted CirA synthesis through direct pairing with *cirA* mRNA.

RyhB protects cirA mRNA from RNase E degradation

Since RNase E is known to be the main endonuclease responsible for RNA turnover in *E. coli* (Belasco, 2010), we explored the possibility that RyhB protected *cirA* mRNA from RNase E degradation. Two different mutants of RNase E were used and their effect on *cirA* transcript levels in the presence or absence of RyhB expression was investigated. One mutant (*rne131*) lacked residues 586–1061 that constitute the C-terminal domain involved in interaction with other components of the RNA degradosome and with Hfq (Kido *et al*, 1996; Vanzo *et al*, 1998). Results showed that *cirA* mRNA levels were low in Δ*ryhB* as in *rne131* Δ*ryhB* cells (Supplementary Figure S2A, lanes 2 and 4). These data led us to conclude that the degradation of *cirA* mRNA in the absence of RyhB did not require interaction of RNase E with the RNA degradosome components or with Hfq. The other mutant (*rne-3071*) was a thermosensitive allele where RNase E becomes inactive at non-permissive temperature (44°C for 15 min) (McDowall *et al*, 1993). In these experiments, *cirA* transcript accumulated at levels similar to WT in the absence of RyhB expression when RNase E was inactivated following a 15-min exposure of the *rne-3071* Δ*ryhB* strain at 44°C (Supplementary Figure S2B, lanes 6 and 8). These data indicate that RNase E was responsible for the turnover of *cirA* mRNA in the absence of RyhB.

RyhB stabilizes cirA mRNA through translational activation

RNase E is considered to be responsible for the rapid decay of translationally impaired mRNAs (Arnold *et al*, 1998; Deana and Belasco, 2005). We thus tested the possibility that RyhB protected *cirA* mRNA from RNase E degradation by activating its translation, as reported in the case of *shiA* mRNA (Prévost *et al*, 2007). This possibility was investigated by first comparing the effect of RyhB on the activity of *cirA′-lacZ* transcriptional fusion and *cirA′-′lacZ* translational fusion. Results demonstrated that RyhB expression resulted in a 1.6-fold activation of transcriptional *cirA′-lacZ* fusion and a 3.8-fold activation of translational *cirA′-′lacZ* fusion (Figure 4A). Moreover, we compared the activities of both fusions in WT and Δ*ryhB* cells grown in an iron-free minimal medium. The absence of *ryhB* resulted in a 2.2-fold decrease in activity for transcriptional *cirA′-lacZ* fusion and a 4.1-fold decrease in activity for translational *cirA′-′lacZ* fusion (Figure 4B). The differential effect of RyhB expression on translational fusion as compared to transcriptional fusion suggested that RyhB activated *cirA* translation.

We next constructed the *cirAmutAUG′-lacZ* transcriptional fusion in which the *cirA* initiation codon AUG was changed to CUG to prevent translation initiation. As expected, β-galactosidase activity was not detected in *cirAmutAUG′-′lacZ* translational fusion (data not shown). RyhB expression did not activate *cirAmutAUG′-lacZ* transcriptional fusion as opposed to a 1.5-fold activation observed in the case of *cirA′-lacZ* fusion (Figure 4C). Furthermore, when cells were grown in minimal iron-free medium, there was no effect on *cirAmutAUG′-lacZ* transcriptional fusion whether RyhB was present or not (WT/Δ*ryhB* = 0.9) as opposed to a 2.1-fold increase in *cirA′-lacZ* activity observed in WT cells as compared to Δ*ryhB* cells (Figure 4D). *cirAmutAUG′-lacZ* transcriptional fusion activity was six-fold lower than *cirA′-lacZ* fusion. We attributed the decrease in β-galactosidase activity to the instability of untranslated *cirAmutAUG* mRNA. Our results suggested that RyhB pairing with *cirA* mRNA increased translation, protected the ORF from RNase E degradation and therefore resulted in accumulation of full-length *cirA* mRNA.

Hfq represses cirA translation

Previously, we have reported that Hfq repressed *shiA* mRNA translation when RyhB was not expressed (Prévost *et al*, 2007). We thus investigated whether Hfq played a similar role in *cirA* activation by RyhB. Northern blots were used to monitor *cirA* transcript levels in Δ*hfq* and Δ*hfq* Δ*ryhB* cells. Results revealed that *hfq* inactivation in a Δ*ryhB* background fully restored *cirA* expression (Figure 5A, lanes 2 and 4), as observed in the case of *shiA* mRNA. In agreement with previous reports (Wassarman *et al*, 2001; Holmqvist *et al*, 2010), we observed that Hfq had an effect on OmrA/B expression as revealed by the fact that both sRNAs were barely detectable in Δ*hfq* and Δ*hfq* Δ*ryhB* cells in comparison with WT and Δ*ryhB* cells (Figure 5A, lanes 1 and 2, and lanes 3 and 4). With respect to this observation, the WT levels of *cirA* mRNA in Δ*hfq* Δ*ryhB* cells could be attributed to decreased OmrA/B repression. However, this is unlikely because *omrAB* inactivation in a Δ*ryhB* background failed to increase levels of *cirA* mRNA (Supplementary Figure S3, lanes 2 and 4).

We next monitored the activity of transcriptional *cirA′-lacZ* and translational *cirA′-′lacZ* fusions in Δ*hfq* Δ*ryhB* cells in comparison to Δ*ryhB* cells. Results showed that inactivation of *hfq* in Δ*ryhB* cells restored WT levels of activity in both cases, suggesting that RyhB activated *cirA* mRNA translation by counteracting Hfq repression (Figure 5B). The greater effect of *hfq* inactivation on *cirA′-′lacZ* translational fusion (3.5-fold increase) as opposed to *cirA′-lacZ* transcriptional

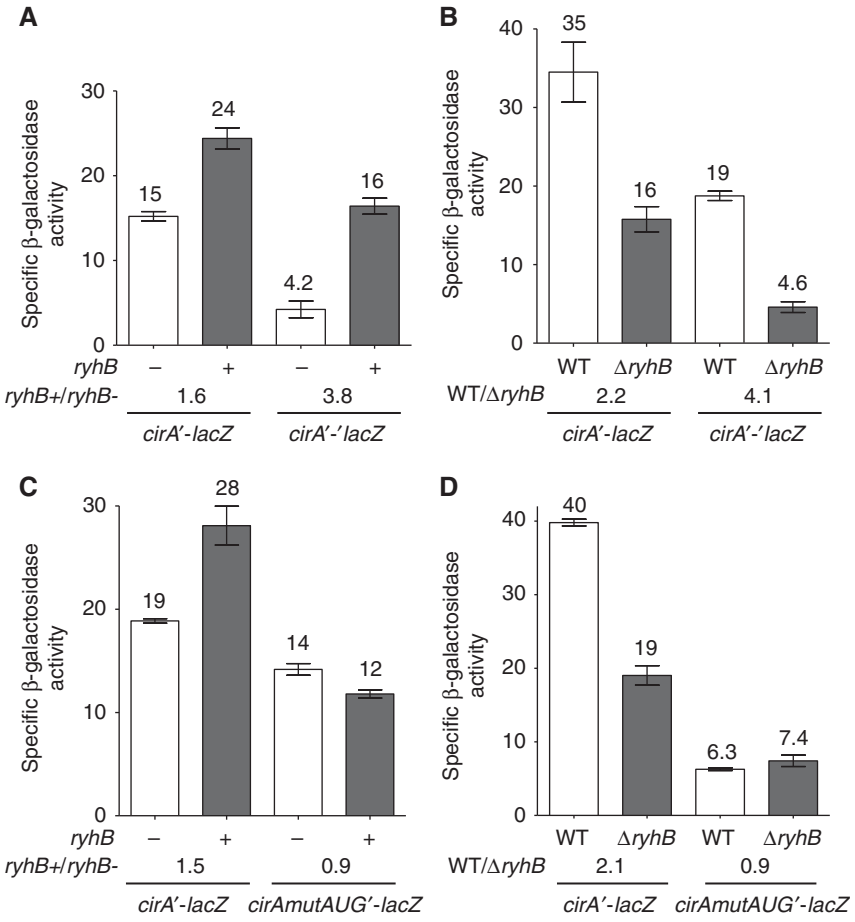

Figure 4 RyhB protects *cirA* mRNA from degradation by activating its translation. (**A**) Effect of arabinose-induced RyhB on *cirA′-lacZ* transcriptional fusion and on *cirA′-′lacZ* translational fusion in a Δ*fur* Δ*ryhB* background. Cells were grown in LB medium and 0.1% arabinose was added at an OD_{600} of 0.1. Specific β-galactosidase activity from three independent cultures was then measured 3 h later. Mean and standard deviation (s.d.) values are shown. Empty vector pNM12 was used as a control. (**B**) β-Galactosidase assay of *cirA′-lacZ* transcriptional fusion and *cirA′-′lacZ* translational fusion in WT and Δ*ryhB* cells grown in M63 iron-free glucose minimal medium at an OD_{600} of 0.6. Specific β-galactosidase activity from three independent cultures was measured. Mean and s.d. values are shown. (**C**) Effect of arabinose-induced RyhB on *cirAmutAUG′-lacZ* transcriptional fusion in a Δ*fur* Δ*ryhB* background. Cells were grown in LB medium and 0.1% arabinose was added at an OD_{600} of 0.1. Specific β-galactosidase activity from three independent cultures was then measured 3 h later. Mean and s.d. values are shown. Empty vector pNM12 was used as a control. (**D**) β-galactosidase assay of *cirAmutAUG′-lacZ* transcriptional fusion in WT and Δ*ryhB* cells grown in M63 iron-free glucose minimal medium at an OD_{600} of 0.6. Specific β-galactosidase activity from three independent cultures was measured. Mean and s.d. values are shown.

fusion (2.2-fold increase) suggested that *cirA* repression by Hfq occurred at the translational level.

The possibility that RyhB activated *cirA* solely by antagonizing Hfq repression would be incompatible with its capacity to further activate *cirA* in the absence of Hfq. However, pulse expression of RyhB in the Δ*fur* Δ*ryhB* Δ*hfq* background resulted in a 1.8-fold increase in *cirA* mRNA levels within 10 min, indicating that RyhB was able to activate *cirA* in the absence of Hfq (Figure 5C, lanes 5 and 6, and lanes 7 and 8). To determine whether this increase in *cirA* mRNA resulted from translational activation, we monitored RyhB effect on *cirA′-lacZ* transcriptional and *cirA′-′lacZ* translational fusions. Results demonstrated that inactivation of *hfq* in the Δ*fur* Δ*ryhB* background resulted in a 2.1-fold increase in *cirA′-lacZ* transcriptional activity and in a 4.8-fold increase in *cirA′-′lacZ* translational activity (Figure 5D). These results were similar to the effect of RyhB on both fusions in the Δ*fur* Δ*ryhB* background (2-fold activation for *cirA′-lacZ* transcriptional fusion and 4.6-fold activation for *cirA′-′lacZ* translational fusion), in agreement with previous results (Figure 5B). These data confirmed that RyhB expression counteracted the repressive effect of Hfq on *cirA* mRNA. However, RyhB expression in Δ*fur* Δ*ryhB* Δ*hfq* cells did not result in a significant increase in *cirA′-lacZ* transcriptional activity but a small but significant 1.1-fold increase in *cirA′-′lacZ* translational activity (Figure 5D). These results contrasted with those of northern blot experiments (Figure 5C) where a 1.8-fold increase in *cirA* transcript levels was observed following RyhB expression. Together, these results suggested that Hfq destabilized *cirA* mRNA through translational repression and that RyhB expression abolished this repression.

Hfq inhibits 30S ribosomal subunit binding to cirA mRNA upon translation initiation

We next sought to decipher the mechanism by which Hfq repressed *cirA* mRNA translation. Previous studies had unveiled the capacity of Hfq to inhibit 30S translation initiation complex formation on some mRNAs through binding to

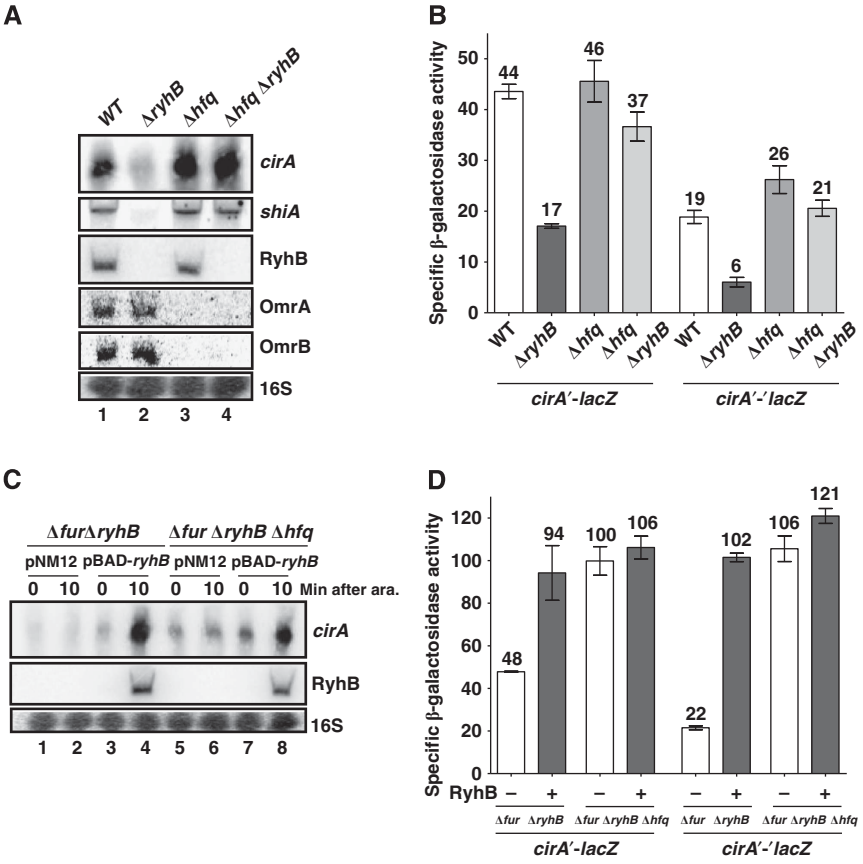

Figure 5 Hfq represses *cirA* mRNA translation. (**A**) Northern blot analysis of Hfq effect on *cirA* mRNA levels. Strains EM1055 (WT), EM1238 (Δ*ryhB*), EM1265 (Δ*hfq*) and KP111 (Δ*hfq* Δ*ryhB*) were grown in M63 iron-free glucose minimal medium at an OD_{600} of 0.6 and total RNA was extracted. Probes complementary to *cirA* and *shiA* open reading frames (ORFs) were used. (**B**) β-Galactosidase assay of *cirA′-lacZ* transcriptional fusion and *cirA′-′lacZ* translational fusion in Δ*hfq* and Δ*hfq* Δ*ryhB* cells grown in M63 iron-free glucose minimal medium at an OD_{600} of 0.6. Specific β-galactosidase activity from three independent cultures was measured. Mean and standard deviation (s.d.) values are shown. (**C**) Northern blot analysis of arabinose-induced RyhB effect on *cirA* mRNA levels in Δ*fur* Δ*ryhB* Δ*hfq* cells. Strains HS506 (Δ*fur* Δ*ryhB*) and HS518 (Δ*fur* Δ*ryhB* Δ*hfq*), each carrying pBAD-*ryhB* or control plasmid pNM12, were grown in M63 iron-free glycerol minimal medium. Arabinose (0.1%) was added at an OD_{600} of 0.3 and total RNA was extracted 10 min later. A probe complementary to *cirA* ORF was used. (**D**) Effect of arabinose-induced RyhB on *cirA′-lacZ* transcriptional fusion and *cirA′-′lacZ* translational fusion in a Δ*fur* Δ*ryhB* Δ*hfq* background. Cells were grown in M63 iron-free glycerol minimal medium and 0.1% arabinose was added at an OD_{600} of 0.1. Specific β-galactosidase activity from three independent cultures was then measured 3 h later. Mean and s.d. values are shown. Empty vector pNM12 was used as a control. Source data for this figure is available on the online supplementary information page.

AU-rich single-stranded regions located in the vicinity of the TIR and acting as translational enhancers (Vytvytska *et al*, 2000; Desnoyers and Massé, 2012). To determine whether Hfq could repress *cirA* translation through this mechanism, we first performed toeprinting experiments to study the effect of Hfq on 30S binding to *cirA* mRNA. We used the Hfq-independent *lpp* transcript (Vytvytska *et al*, 1998, 2000) as a control (Supplementary Figure S4A and B). Results indicated that addition of purified 30S ribosomal subunits and $tRNA^{fmet}$ to *cirA* mRNA (0.2 μM) resulted in a strong block of reverse transcription at positions +15/+16 downstream of the AUG start codon (Figure 6A). These observations were consistent with the formation of a translation initiation complex on *cirA* mRNA. Addition of increasing amounts of purified Hfq (200 nM) resulted in a 2.2-fold inhibition of initiation complex formation (Hfq:*cirA* molar ratio, 1:1) and in near complete inhibition at high concentration (500 nM) of Hfq (Hfq:*cirA* molar ratio, 2.5:1). These results suggested that Hfq binding to *cirA* mRNA may be sufficient to prevent translation initiation *in vivo*. As expected, higher concentrations of Hfq were required to prevent ribosome binding to *lpp* mRNA (Supplementary Figure S4A).

We next performed enzymatic and chemical probing using RNase I (cleaves unpaired nucleotides) and PbAc to identify potential Hfq binding sites in the 5′-UTR of *cirA* mRNA. Addition of increasing amounts of Hfq to 5′-end-labelled *cirA* mRNA resulted in protection of nucleotides −105 to −91 from RNase I cleavage (Figure 6B, Hfq I site, lane 6 and lanes 7–9). This region is AU-rich and single-stranded, according to its susceptibility to RNase I cleavage (Figure 6B, lane 6, Hfq I site). These properties were consistent with previous descriptions of Hfq binding sites (Lorenz *et al*, 2010; Balbontín *et al*, 2010). Protection of nucleotides −63 to −53 from RNase I cleavage was also observed at high concentrations of Hfq (Figure 6B, lanes 6 and lanes 7–9) that may result from Hfq binding to site I.

Interestingly, incubation of *cirA* with Hfq resulted in a weak but noticeable protection of nucleotides +4 to +6 from RNase I cleavage (Figure 6B, Hfq III site, lanes 6–9). These nucleotides are also protected from PbAc cleavage in

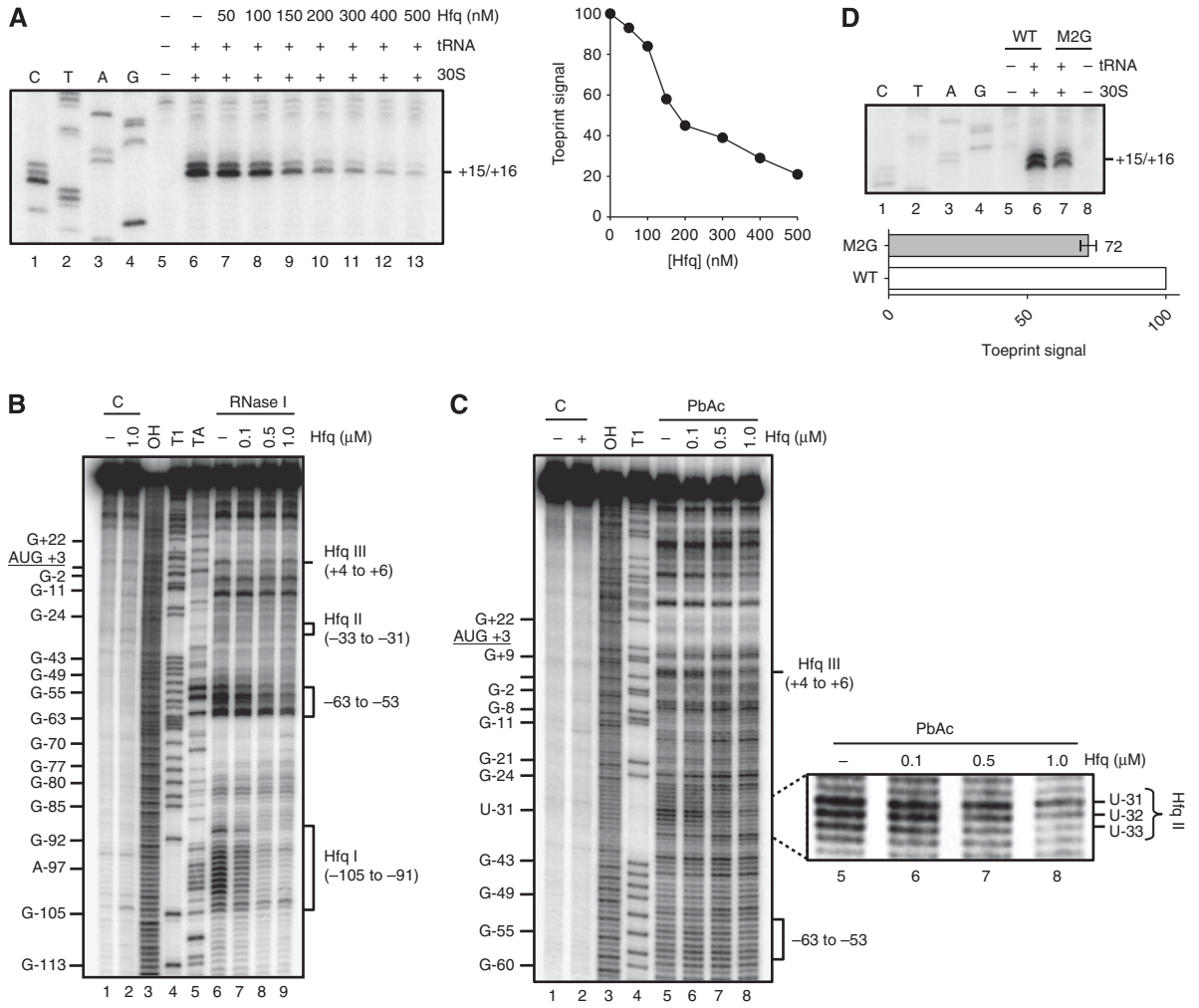

Figure 6 Hfq represses 30S ribosomal subunit binding to *cirA* mRNA upon translation initiation. (**A**) Toeprint analysis of Hfq effect on 30S ribosomal subunit binding to *cirA* mRNA (200 nM) upon translation initiation. Unlabelled *cirA* mRNA was incubated in the presence of the indicated amounts of purified Hfq protein. Positions +15/+16 relative to *cirA* AUG start codon are indicated. CTAG refers to sequencing ladders. Toeprint signals were quantified by densitometry and data are reported in arbitrary units. (**B**) RNase I probing of Hfq binding sites on *cirA* mRNA. 5′-end-labelled *cirA* mRNA (nucleotides −173 to +78 relative to the AUG start codon) was incubated in the presence of the indicated amounts of purified Hfq protein before addition of RNase I. Hfq I, Hfq II, and Hfq III refer to Hfq binding sites I, II, and III (see Figure 2). C, non-reacted controls; OH, alkaline ladder; T1, RNase T1 ladder (guanine residues); TA, RNase TA ladder (adenine residues). (**C**) PbAc probing of Hfq binding sites on *cirA* mRNA. 5′-end-labelled *cirA* mRNA (nucleotides −173 to +78 relative to the AUG start codon) was incubated in the presence of the indicated amounts of purified Hfq protein before addition of PbAc (5 mM). Hfq II and Hfq III refer to Hfq binding sites II and III (see Figure 2). Some guanine and adenine positions are given for clarity. C, non-reacted controls; OH, alkaline ladder; T1, RNase T1 ladder (guanine residues). The region corresponding to Hfq binding site II (Hfq II) is enlarged to illustrate protection from PbAc cleavage of nucleotides −33 to −31 following addition of Hfq. (**D**) Toeprint analysis of 30S ribosomal subunit binding to *cirA*M2G mRNA. Unlabelled *cirA* and *cirA*M2G mRNAs (0.2 μM final) were incubated in the presence of 30S ribosomal unit and $tRNA^{fmet}$. Positions +15/+16 relative to *cirA* and *cirA*M2G AUG start codons are indicated. CTAG refers to sequencing ladders. Toeprint signals of two independent experiments were quantified by densitometry and normalized to WT toeprint signal (lane 6). Data are reported in arbitrary units. Mean and standard deviation (s.d.) values of duplicate experiments are shown. Source data for this figure is available on the online supplementary information page.

the presence of Hfq (Figure 6C, Hfq III site, lanes 5–8). This region is U-rich and single-stranded according to secondary structure prediction (Figure 2) and to the susceptibility of nucleotides +4 to +6 to RNase I (Figure 6B, Hfq III site, lane 6) and PbAc (Figure 6C, Hfq III site, lane 5) cleavages in the absence of Hfq. Binding of this U stretch by Hfq could potentially hamper 30S binding to the AUG start codon of *cirA* mRNA upon translation initiation (Figure 6A).

Nucleotides −33 to −31, which are part of an AU-rich region, were also protected from PbAc cleavage upon addition of Hfq (Figure 6C, Hfq II site, lanes 5–8). These nucleotides were predicted to be part of a stem-loop structure (Figure 2, SL3, nucleotides A-40 to G+12), consistent with their protection from RNase I cleavage (Figure 6B, Hfq II site, lane 6). These nucleotides (−33 to −31) are also part of an AU-rich region (nucleotides A-35 to U-26) located a few nucleotides upstream of the Shine-Dalgarno sequence, suggesting that this region acts as a translational enhancer. To investigate this, we constructed a *cirA*M2G mRNA in which nucleotides U-32 and U-31 were replaced by two guanine residues (Figure 2) and 30S binding was monitored by toeprinting. Results showed that there was ∼30% less binding of 30S to *cirA*M2G mRNA than to *cirA* mRNA (Figure 6D,

lanes 6 and 7), suggesting an important role of region A-35 to U-26 in translation initiation.

Despite the fact that Hfq I site was highly AU-rich (Figure 2), we did not expect this region to act as a translational enhancer. The Hfq I site is too far upstream of the Shine-Dalgarno sequence in comparison with translational enhancer elements previously described (Hook-Barnard *et al*, 2007; Desnoyers and Massé, 2012). Indeed, replacement of nucleotides A-100 and A-98 for cytosine residues (*cirA*ML, Supplementary Figure S5A) did not result in reduced formation of 30S translation initiation complex (Supplementary Figure S5B, lanes 7 and 8). Taken together, our results suggested that Hfq may repress *cirA* mRNA translation by preventing 30S initiation complex formation through binding in the vicinity of the AUG start codon (Hfq III site) and/or to a translational enhancer element (Hfq II site) located a few nucleotides upstream of the Shine-Dalgarno sequence.

RyhB promotes 30S ribosomal subunit binding to cirA mRNA in the presence of Hfq

Data presented above (Figure 4) strongly suggested that RyhB stabilized *cirA* mRNA through translational activation. We hypothesized that RyhB pairing with *cirA* 5′-UTR would result in increased 30S binding to the AUG start codon upon translation initiation. Unexpectedly, addition of increasing amounts of RyhB to *cirA* mRNA (0.2 μM) resulted in a 12% inhibition of initiation complex formation in the presence of RyhB (0.4 μM, RyhB:*cirA* molar ratio, 2:1) and a 30% inhibition with a higher concentration (0.8 μM) of RyhB (RyhB:*cirA* molar ratio, 4:1) (Supplementary Figure S6, lane 6 and lanes 8–10). This negative effect of RyhB on 30S binding to *cirA* mRNA appeared to be pairing specific since addition of RyhB1 did not repress initiation complex formation (Supplementary Figure S6, lane 6 and lanes 12 and 14).

As a follow-up to results presented above (Figure 5B) that suggested that RyhB activated *cirA* by counteracting Hfq translational repression, we tested the effect of RyhB on 30S binding to *cirA* mRNA in the presence of Hfq. Addition of Hfq (150 nM, Hfq:*cirA* molar ratio, 0.75:1) resulted in 30% inhibition of 30S binding to *cirA* mRNA (Figure 7A, lanes 6 and 8). Consistent with the *in vivo* data, addition of RyhB (150 nM) in the presence of Hfq (Hfq:RyhB:*cirA* molar ratio, 0.75:0.75:1) resulted in a 60% increase in the toeprint signal (Figure 7A, lanes 8 and 10), whereas addition of the same amount of RyhB1 only results in a 25% increase in 30S binding (Figure 7A, lanes 8 and 12). The weak RyhB1-dependent activation may be attributable to Hfq displacement from *cirA* mRNA via RyhB1 poly(U) tail, which has previously been shown to bind Hfq with high affinity (Otaka *et al*, 2011). We could not exclude the possibility that this titration effect may contribute to RyhB-positive effect on 30S binding to *cirA* mRNA (Figure 7A, lanes 8 and 10). However, the fact that RyhB induced stronger toeprint signals than those observed upon addition of RyhB1 (Figure 7A, lanes 10 and 12), strongly suggested that the RyhB-dependent activation was base pairing specific. Moreover, RyhB did not affect ribosome binding to *lpp* mRNA (negative control) in the presence of Hfq (Supplementary Figure S4B, compare lanes 8 and 10). Taken together, toeprinting data supported the interpretation that RyhB directly promoted translational initiation complex formation on *cirA* mRNA in the presence of Hfq.

We next investigated the mechanism by which RyhB stimulated ribosome binding to *cirA* mRNA in the presence of Hfq upon translation initiation. Previous studies of sRNA-mediated translational activation (e.g., RyhB-*shiA*,

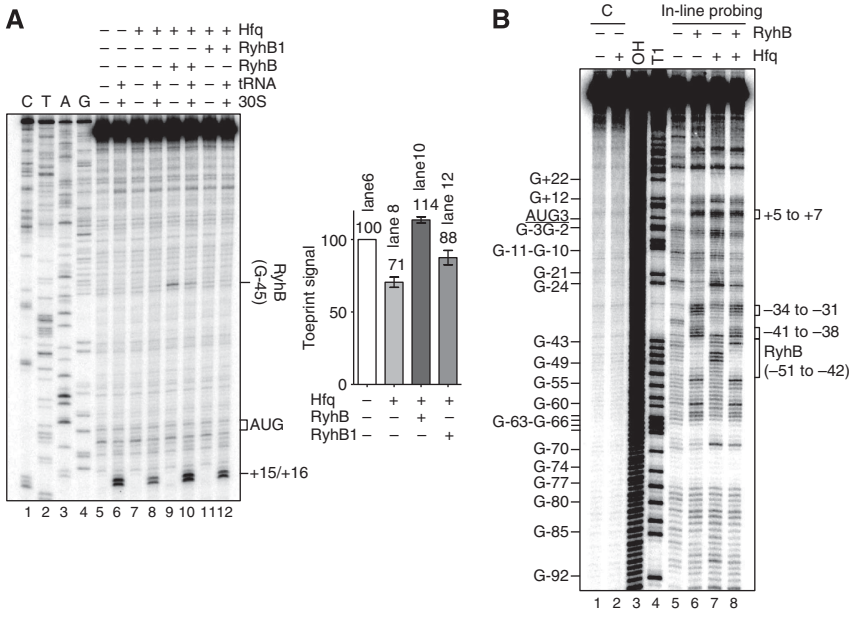

Figure 7 RyhB promotes 30S ribosomal subunit binding to *cirA* mRNA in the presence of Hfq. (**A**) Toeprint analysis of RyhB and RyhB1 effects on 30S ribosomal subunit binding to *cirA* mRNA in the presence of Hfq upon translation initiation. Unlabelled *cirA* mRNA (0.2 μM final) was incubated in the presence of Hfq (0.15 μM) and RyhB (0.15 μM) or RyhB1 (0.15 μM). Positions + 15/ + 16 relative to *cirA* AUG start codon are indicated. CTAG refers to sequencing ladders. Toeprint signals of two independent experiments were quantified by densitometry and normalized to the toeprint signal in lane 6. Data are reported in arbitrary units. Mean and standard deviation (s.d.) values of duplicate experiments are shown. (**B**) In-line probing analysis of Hfq and RyhB effects on *cirA* mRNA. 5′-end-labelled *cirA* mRNA (nucleotides − 173 to + 78 relative to the AUG start codon) was incubated for 40 h in the presence of Hfq (0.3 μM) and RyhB (1 μM). Some guanine positions are illustrated for clarity. C, non-reacted controls; OH, alkaline ladder; T1, RNase T1 ladder (guanine residues). Source data for this figure is available on the online supplementary information page.

DsrA-*rpoS*, and GlmZ-*glmS*) have shown that sRNA pairing with its target mRNA usually results in the disruption of an inhibitory structure that sequesters the Shine-Dalgarno sequence (Fröhlich and Vogel, 2009). We performed in-line probing to determine whether *cirA* regulation by RyhB and Hfq occurred through a similar mechanism. This technique exploits the natural susceptibility of unpaired and unstructured nucleotides of RNA to spontaneous cleavage in solution (Wakeman and Winkler, 2009). Results showed that RyhB pairing with 5′-end-labelled *cirA* mRNA in the presence of Hfq (confirmed by the cleavage protection of nucleotides −51 to −42) (Figure 7B, lanes 7 and 8) resulted in increased cleavage of nucleotides −41 to −38 and −34 to −31 (Figure 7B, lanes 7 and 8). Notably, these secondary structure changes are also observed when RyhB is added in the absence of Hfq (compare lanes 5 and 6), suggesting that they do not require Hfq to occur. These RyhB effects on *cirA* mRNA secondary structure were further confirmed by enzymatic and chemical probing (Supplementary Figure S7). Altogether, these structural changes showed that RyhB pairing with *cirA* mRNA in the presence of Hfq promoted the partial unfolding of SL3 and that resulted in increased accessibility of region −35 to −26, predicted to be bound by Hfq (Figure 2, Hfq II; Supplementary Figure 6B, C) and to act as a potential translational enhancer (Figure 6D). Based on the bulk of these results, it was predicted that this region was more accessible to 30S subunit upon translation initiation.

The addition of RyhB in the absence of Hfq resulted in cleavage induction of nucleotides +5 to +7 (Figure 7B, lanes 5 and 6), which was previously characterized as a Hfq binding site (Figure 2, Hfq III). Unexpectedly, cleavage of this region was observed when *cirA* mRNA was incubated with Hfq alone (Figure 7B, lanes 5 and 7). This induced cleavage may result from residual RNase activity in the Hfq preparation (Supplementary Figure S8, lanes 1 and 2). However, it is more probable that the high susceptibility of region +5 to +7 to cleavage upon incubation with RyhB and Hfq (Figure 7B, lane 8) may be in large part attributable to structural changes specific to RyhB pairing, as RyhB alone promoted the same cleavage intensity in this region (Figure 7B, lanes 6 and 8). These data then suggested that RyhB pairing with *cirA* mRNA in the presence of Hfq resulted in the unfolding of Hfq III region (nucleotides +4 to +6), as it was shown for Hfq II. Since this region is located immediately downstream of the AUG start codon, increased accessibility of this region upon RyhB pairing may stimulate initiation complex formation. Unexpectedly, the structure of the Shine-Dalgarno region (nucleotides −11 to −7) remained unchanged upon RyhB pairing with *cirA* mRNA in the absence or in the presence of Hfq (Figure 7B, lane 5 and lane 6, lane 7 and lane 8), thereby discarding the possibility that RyhB may activate *cirA* mRNA translation by making the Shine-Dalgarno more accessible to the ribosome.

Taken together, results described above strongly suggested that RyhB pairing with *cirA* mRNA resulted in increased accessibility of regions predicted to be targeted by Hfq to repress translation when RyhB was not expressed (Hfq II and Hfq III sites). Indeed, when we mutated the Hfq II site (mutant M2G), we observed a significant decrease in expression of *cirA′-′lacZ* translational fusion (Supplementary Figure S9). Overall, the data provided a plausible mechanism underlying the increased ribosome binding to *cirA* mRNA upon RyhB pairing in the presence of Hfq.

RyhB promotes colicin Ia sensitivity through cirA activation

RyhB was expected to modulate colicin sensitivity upon iron starvation by activating *cirA* translation because colicin Ia is one of the main ligands bound by CirA. WT cells that accumulate high levels of *cirA* mRNA under conditions of iron starvation should be sensitive to colicin treatment as opposed to Δ*ryhB* cells that are expressing low levels of *cirA* mRNA. We monitored the growth of WT, Δ*ryhB* and Δ*cirA* cells in an iron-free minimal medium in the presence or absence of colicin Ia (added at early exponential phase). As expected, WT cells growth was impaired when colicin Ia was added to the medium (Figure 8). In contrast, the growth of Δ*ryhB* and Δ*cirA* cells was not significantly affected. We explain the observed recovery phenotype of WT + colicin by the active division of a small cell population that was not exposed to colicins at the beginning of the treatment. No suppressor mutations conferring colicin Ia resistance were observed during the course of the experiment (Supplementary Figure S10).

Because the siderophore DHB is an additional substrate of CirA, we set up a series of experiments to determine whether prebinding of DHB to CirA could prevent the binding of colicin Ia and protect WT cells from the bactericidal effect of colicin Ia. Results demonstrated that the addition of DHB 30 min before colicin Ia treatment of WT cells conferred nearly complete resistance to colicin Ia (Figure 8). Taken together, these data confirmed that RyhB promoted colicin Ia sensitivity under conditions of iron starvation by activating *cirA* translation.

Discussion

Results reported here unveiled key elements of a complex regulatory network controlling the cellular sensitivity to the antibiotic colicin Ia in an iron-dependent manner (Figure 9). Our data support the interpretation that, under conditions of iron sufficiency, Fe^{2+}-Fur (active Fur) repressed *cirA* and *ryhB* transcription, which resulted in low levels of CirA. However, under conditions of iron starvation, Fur became inactive and *cirA* and *ryhB* were actively transcribed. Strikingly, although *cirA* mRNA was expressed, Hfq binding to sites II and III prevented formation of the translation initiation complex, leading to rapid *cirA* destabilization by RNase E. Hfq-induced translational repression was relieved only when sRNA RyhB base paired with *cirA* mRNA. RyhB allowed translation initiation of *cirA* mRNA by promoting structural changes that increased the accessibility of ribosomal subunit 30S to sites II (translation enhancer) and III (RBS). Translational activation of *cirA* mRNA resulted in increased accumulation of CirA protein in the outer membrane, thereby making cells sensitive to the antibiotic colicin Ia.

Comparison with other positive sRNA-dependent regulations

One may assume that the regulation of *cirA* mRNA by RyhB and Hfq is highly similar to other cases of sRNA-mediated translational activation previously characterized

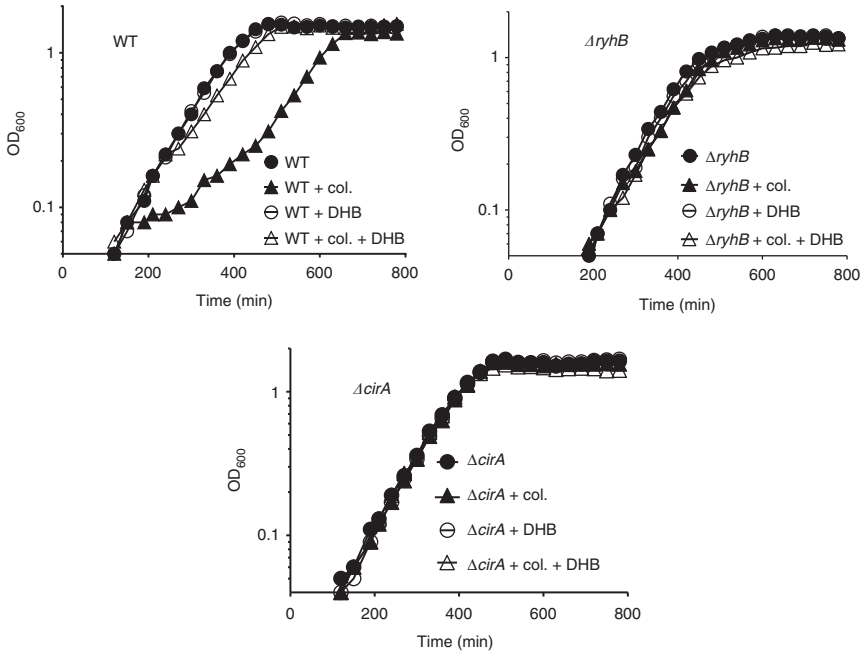

Figure 8 RyhB expression promotes colicin Ia sensitivity under conditions of iron starvation. Strains EM1055 (WT), EM1238 (Δ*ryhB*), and HS221 (Δ*cirA*) were grown in M63 iron-free glucose minimal medium and cleared colicin Ia lysate was added at an OD_{600} of 0.1. When needed, 2,3-dihydroxybenzoic acid (DHB, 33 μM) was added 30 min before addition of colicin Ia. For a determination of the levels of RyhB and *cirA* RNAs performed under the same growth conditions, please refer to Figure 1C.

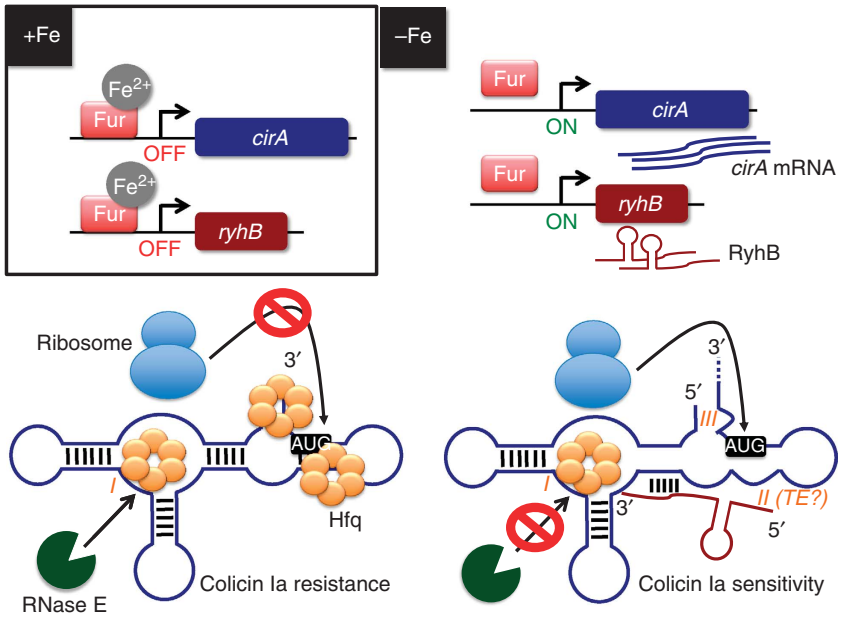

Figure 9 Working model for RyhB-mediated translational activation of *cirA* mRNA (see the text for details). Fe^{2+}, ferrous iron; TE, translational enhancer. I, II, and III refer to Hfq binding sites I, II, and III characterized in the study, respectively.

(e.g., RyhB-*shiA*; DsrA-*rpoS*; ans GlmZ-*glmS*). In such instances, sRNA pairing with the target mRNA typically results in the disruption of a secondary structure that is detrimental to translation initiation (Fröhlich and Vogel, 2009). However, some key differences highlight each mechanism from the others. First, while Hfq represses *cirA* and *shiA* translation when RyhB is not expressed, it does not seem to be the case for *rpoS* and *glmS*. Indeed, the *hfq* mutant strain does not exhibit increased levels of *rpoS* and *glmS* translation under conditions of low DsrA and GlmZ expression, respectively (Sledjeski *et al*, 2001; Urban and Vogel, 2008). Second, RyhB and Hfq are not required for the translation of *cirA* and *shiA*. In other words, the secondary structure of both mRNAs is not predicted to prevent translation initiation, according to *in vitro* and *in vivo* data. Similar levels of 30S binding to *cirA* mRNA were observed whether RyhB and Hfq were present or not (Figure 7A). Moreover, *cirA* and *shiA* transcripts accumulated to WT levels in Δ*hfq* Δ*ryhB* cells

(Figure 5A) and the levels of *cirA* and *shiA* translation were identical to WT cells in a Δ*hfq* Δ*ryhB* background (Figure 5B; Prévost *et al*, 2007). These results were in marked contrast with those of DsrA-*rpoS* and GlmZ-*glmS* regulations in which case sRNA and Hfq have been shown to be essential for translation of the target mRNA (Sledjeski *et al*, 2001; Urban and Vogel, 2008; McCullen *et al*, 2010). Third, whereas RyhB-*shiA*, DsrA-*rpoS* and GlmZ-*glmS* translational activations occurred through increased accessibility of the Shine-Dalgarno sequence following the sRNA pairing (Prévost *et al*, 2007), it did not appear to be the case for RyhB-*cirA* regulation.

Indeed, no structural changes in the Shine-Dalgarno region were observed upon RyhB pairing with *cirA* mRNA in the presence or in the absence of Hfq (Figure 7B; Supplementary Figure S7). Considering that *cirA* mRNA can be translated to WT levels in the absence of RyhB and Hfq (Figure 5B), we may assume RBS to be available for ribosome binding upon translation initiation, which is supported by probing data (Supplementary Figure S7B, lane 5; note the high susceptibility of nucleotides G-11, G-10, and G-8 to RNase T1 cleavage) and toeprinting experiments (Figure 7A; Supplementary Figure S6). Remarkably, most structural changes observed upon RyhB pairing to *cirA* mRNA occurred in regions targeted by Hfq for translational repression (sites II and III, see Figure 2). This result suggested that RyhB action may aim to dislodge Hfq from these sites (discussed below) instead of increasing ribosome access to the Shine-Dalgarno sequence. The incapacity of RyhB to increase 30S binding to *cirA* mRNA in the absence of Hfq further supported this hypothesis (Supplementary Figure S6).

Antagonistic regulation of cirA translation by Hfq and RyhB

Our work demonstrated a situation in which RyhB activated *cirA* translation by preventing Hfq binding to a potential translational enhancer element (site II, see Figure 2). To our knowledge, a similar mechanism of sRNA-mediated gene activation has not yet been characterized. The presence of AU-rich sequences located several nucleotides upstream of the Shine-Dalgarno sequence has been reported to enhance translation and to stabilize transcripts (Zhang and Deutscher, 1992; Hook-Barnard *et al*, 2007). These translational enhancer elements have been shown to increase interaction with ribosomal protein S1 (Boni *et al*, 1991; Komarova *et al*, 2002) that typically recognizes AU-rich single-stranded sequences (Ringquist *et al*, 1995; Hajnsdorf and Boni, 2012). We predict the AU-rich region −35 to −26 of *cirA* mRNA that we identified as a Hfq binding site (Hfq site II) to act as a translational enhancer, given its close proximity to the Shine-Dalgarno sequence (Figure 2) and the high accessibility of nucleotides −33 to −31, according to PbAc probing (Figure 6C, lane 5). Moreover, mutation of nucleotides U-31 and U-32 to guanines reduced 30S binding by 30% (Figure 6D). This decrease corresponded to the level of repression observed upon incubation of *cirA* mRNA with Hfq (Figure 7A), suggesting that most of the translational repression mediated by Hfq could occur through binding to these nucleotides. Our findings are in agreement with these observations and suggest a potential role of Hfq II site as a translational enhancer.

Although the 30% repression of 30S binding observed upon incubation of *cirA* mRNA with Hfq is moderate, we suggest that it is sufficient to repress translation and to promote *cirA* transcript destabilization. The 60% activation by RyhB observed in toeprint experiments (Figure 7A) would then allow translation to resume and *cirA* mRNA to accumulate. Further repression of ribosome binding observed with higher concentrations of Hfq (Figure 6A) may not occur *in vivo* due to limiting concentrations of Hfq in the cell (Moon and Gottesman, 2011; Hussein and Lim, 2011). Moreover, the Hfq binding site III (Figure 2, region +4 to +9) of *cirA* mRNA may be critical for translational regulation. Given that any sRNA pairing immediately upstream of the Shine-Dalgarno sequence or within the first five codons of the open reading frame was able to compete directly with initiating ribosomes (Bouvier *et al*, 2008), we would predict Hfq binding to site III to interfere with translation initiation complex formation. Our probing data suggested that Hfq may be dislodged from sites II and III following RyhB pairing (Figure 7B; Supplementary Figure S7). Considering this possibility, we hypothesized that structural changes induced by RyhB upon base pairing with *cirA* mRNA destabilized Hfq interactions with sites II and III, thereby resulting in translational activation.

It is tempting to suggest that structural changes occurring on *cirA* mRNA following RyhB pairing not to have major effects on translation in the absence of Hfq, as suggested by toeprint experiments (Supplementary Figure S6). However, RyhB expression in Δ*hfq* cells resulted in a significant increase in *cirA* mRNA levels (Figure 5C). This Hfq-independent effect of RyhB on *cirA* expression remains elusive. One may assume this activation to result from the subtle 15% increase in *cirA* translation observed upon RyhB expression in the absence of Hfq (Figure 5D) that could be sufficient to stabilize *cirA* mRNA. On the other hand, the possibility of an RyhB-mediated stabilization of *cirA* transcript independent of ribosome protection cannot be excluded.

Introduction of mutations into the Hfq binding site I did not reduce 30S binding to *cirA* mRNA (Supplementary Figure S5), suggesting that this region may not regulate translation initiation. Based on the observation that Hfq greatly stimulated RyhB pairing to *cirA* mRNA *in vitro* (Supplementary Figure S11), we predict Hfq to bind Hfq I site to promote RyhB-*cirA* duplex formation *in vivo*. Upon pairing with *cirA* mRNA, the RyhB poly(U) tail, which was reported to bind Hfq with high affinity (Otaka *et al*, 2011), is oriented towards Hfq site I. Binding of Hfq to both site I and RyhB 3′-end under these conditions could then promote stabilization of the RyhB-*cirA* hybrid, thus allowing sustained translational activation during iron starvation.

A feed-forward loop motif controls colicin sensitivity and iron uptake

The Fur-RyhB-*cirA* regulatory circuit forms a coherent type 2 feed-forward loop in which Fe^{2+}-Fur represses *cirA* and *ryhB* while RyhB activates *cirA* (Supplementary Figure S12). Such a network motif is predicted to delay the induction of the target gene, according to computational modelling on transcription networks (Mangan and Alon, 2003). Application of the model to *cirA* regulation when cells experience iron starvation predicts *cirA* expression to be delayed in comparison to direct regulation by Fe^{2+}-Fur. This would be

logical, considering that once Fur becomes inactive and *cirA* promoter is fully expressed, RyhB synthesis must reach a certain threshold for *cirA* mRNA to be translated and stabilized. Conversely, no lag of repression is expected for transcriptional networks with the same configuration as the Fur-RyhB-*cirA* loop. This prediction may not apply to *cirA* repression, considering the fact that feed-forward loops integrating sRNAs often display altered regulatory dynamics when compared to transcriptional feed-forward loops (Shimoni *et al*, 2007; Beisel and Storz, 2010, 2011). One could imagine that under conditions when cells switch from iron-poor to iron-rich conditions and when Fur becomes active, despite the fact that Fe^{2+}-Fur represses *cirA* and *ryhB* transcription, there are still *cirA* transcripts activated by existing RyhB molecules that were transcribed before Fur repression. Consequently, CirA proteins will be synthesized until the existing pool of *cirA* transcripts becomes exhausted. We would then expect *cirA* repression to be delayed in this context as compared to direct repression by Fe^{2+}-Fur.

Physiological relevance of colicin sensitivity upon iron starvation

Colicins are produced following DNA damages as a result of the SOS response as well as various cellular stresses such as thymine starvation, high temperatures or anaerobiosis (Cascales *et al*, 2007). Under these conditions, colicin-producing strains lyse and released colicins kill surrounding colicin-sensitive cells. Despite the fact that the role of colicins in survival to iron starvation has not yet been addressed, we can speculate colicin sensitivity to confer a selective advantage for the bacterial community when iron is scarce. Cells experiencing iron deficiency and, thereby expressing CirA, would become sensitive to the killing action of colicin Ia and lyse. Then, the released iron could be imported from the environment by the remaining cell population for survival. The DHB molecules expelled in the medium upon cell death could in turn protect the remaining cells from colicin action through competitive binding to CirA, as observed here (Figure 8 in the case of WT cells), thus preventing elimination of the whole bacterial population.

Our work further supports the active role of RyhB in gene activation in addition to its well-known function as a gene silencer. The feed-forward loop by the Fur-RyhB-*cirA* regulatory circuit also unveils a novel type of iron-dependent regulation. To our knowledge, *cirA* is the first Fur-regulated gene to require further post-transcriptional activation by RyhB upon iron starvation that has been characterized so far. Further investigation is warranted to uncover similar type of regulation in the future.

Materials and methods

Strains and plasmids

Derivatives of *E. coli* MG1655 were used in all experiments (Supplementary Table S1). DH5α strain was used for routine cloning procedures. EM1055 (wild type, MG1655 derivative), EM1451 (Δ*ara714 leu*$^+$), EM1455 (Δ*ara714 leu*$^+$ Δ*ryhB*::*cat*), EM1238 (Δ*ryhB*::*cat*), EM1256 (Δ*fur*::*kan*), EM1237 (DY330 [W3110 Δ*lacU169 gal490* λ*cI857* Δ(*cro-bioA*)]), EM1265 [*hfq-1*::Ω(*kan;Bcl1*)], EM1277 (*rne-3071 zce-726*_Tn10), EM1280 (*rne-3071 zce-726*_Tn10 Δ*ryhB*::*cat*), EM1377 (*rne-131 zce-726*_Tn10), KP392 (Δ*fur*::*kan*), KP393 (Δ*fur*::*kan* Δ*ryhB*::*cat*), and JW4130-1 (*rrnB3* Δ*lacZ4787 hsdR514* Δ(*araBAD*)567 Δ(*rhaBAD*)568 *rph-1* Δ*hfq-722*::*kan*) have been described earlier (Yu *et al*, 2000; Massé and Gottesman, 2002; Massé *et al*, 2003; Baba *et al*, 2006; Desnoyers *et al*, 2009; Salvail *et al*, 2010). Strains constructed by P1 transduction were selected for the appropriate antibiotic-resistant marker. Except as otherwise indicated, for cells carrying plasmid pNM12, pBAD-*ryhB*, pBAD-*ryhB1* and pCP20 (see Supplementary Table S2 for a list of plasmids), ampicillin was used at a final concentration of 50 μg/ml. Deletion/insertion mutations in *cirA* (Δ*cirA*::*tet*), *omrAB* (Δ*omrAB*::*tet*), *araB* (Δ*araB*::*kan*) and *fur* (Δ*fur*::*tet*) were constructed by the method described by Yu *et al.* Tetracycline resistance cassette was first amplified by PCR from strain EM1053 (oligos EM215-EM216) (see Supplementary Table S3 for a list of oligonucleotides). The PCR fragment obtained was then amplified with oligos containing sequences that are homologous to the 5′ and 3′ ends of the cassette and sequences homologous to *cirA* (oligos EM1044–EM1045), *omrAB* (oligos EM1599–EM1600), and *fur* (oligos EM1989–EM1990). Flippase recognition target (FRT)-flanked kanamycin resistance cassette was generated by PCR from a DH5α strain harbouring pKD4 plasmid with oligos containing sequences that are homologous to the 5′ and 3′ ends of the cassette and sequences homologous to *araB* (oligos EM1388–EM1389). The resulting PCR products were transformed into EM1237 after induction of λ*red*, according to Yu *et al*, selecting for tetracycline resistance for *cirA* and *omrAB* mutations and for kanamycin resistance for *araB* mutation. Recombinant products were verified by sequencing. Following P1 transduction of *araB::kan*, kanamycin resistance cassette was removed using flippase (Flp) encoding helper plasmid pCP20 as described (Datsenko and Wanner, 2000).

RNA extraction and northern blot analysis

Northern blots were performed as described previously (Desnoyers and Massé, 2012) with some modifications. Total RNA was extracted from cells grown at 37°C or 30°C, for experiments with thermosensitive strains (EM1277 and EM1280), in LB or M63 minimal medium containing glucose or glycerol (0.2%) using the hot phenol procedure (Aiba *et al*, 1981). Arabinose (0.1%), 2,2′-dipyridyl (250 μM) or $FeSO_4$ (5 μM) was added when indicated. Following total RNA extraction, 5–10 μg of total RNA was loaded on polyacrylamide gel (4–6% acrylamide 29:1, 8 M urea) and 15 μg was loaded on agarose gel (1%, 1X MOPS).

Primer extension

Reverse transcription was performed as previously described (Prévost *et al*, 2007).

OMPs analysis

Cells were grown in 50 ml of LB medium to an OD_{600} of 1.0 and 10 ml of culture was harvested and OMPs were extracted as previously described (Morona and Reeves, 1982; Guillier and Gottesman, 2006).

β-Galactosidase assays

Kinetic assays for β-galactosidase activity were performed as described (Prévost *et al*, 2007), using a SpectraMax 250 microtitre plate reader (Molecular Devices).

qRT–PCR analysis

qRT–PCR was performed according to a previous report (Salvail *et al*, 2010).

RNA secondary structure probing

Secondary structure probing was performed as described earlier (Desnoyers *et al*, 2009). In-line probing experiments were performed as previously described (Regulski and Breaker, 2008; Wakeman and Winkler, 2009).

Toeprinting assays

Toeprinting assays were carried out according to a previous report (Salvail *et al*, 2010).

Supplementary data

Supplementary data are available at *The EMBO Journal* Online (http://www.embojournal.org).

Acknowledgements

We would like to thank Charles M Dozois (INRS-Institut Armand-Frappier) for the colicin-producing strains and Eric Cascales (Laboratoire d'Ingénierie des Systèmes Macromoléculaires, CNRS UMR7255), Hanah Margalit (The Hebrew University of Jerusalem), Uri Alon and Avi Mayo (Weizmann Institute of Science) for fruitful discussions. We also thank Fabien Darfeuille (Université Bordeaux Segalen), Karine Prévost and Guillaume Tremblay for excellent technical assistance. This work was funded by an operating grant MOP69005 to EM from the Canadian Institutes for Health Research (CIHR). HS holds an Alexander-Graham-Bell PhD studentship from the Natural Sciences and Engineering Research Council of Canada (NSERC). EM is a Fonds de la Recherche en Santé du Québec (FRSQ) Senior scholar.

Author contributions: HS, M-PC, and EM designed research; HS, M-PC, and JB performed research; HS, M-PC, JB, and EM analysed data; HS and EM wrote the paper.

Conflict of interest

The authors declare that they have no conflict of interest.

References

Aiba H, Adhya S, de Crombrugghe B (1981) Evidence for two functional *gal* promoters in intact *Escherichia coli* cells. *J Biol Chem* **256:** 11905–11910

Andrade JM, Pobre V, Matos AM, Arraiano CM (2012) The crucial role of PNPase in the degradation of small RNAs that are not associated with Hfq. *RNA* **18:** 844–855

Arnold TE, Yu J, Belasco JG (1998) mRNA stabilization by the ompA 5′ untranslated region: two protective elements hinder distinct pathways for mRNA degradation. *RNA* **4:** 319–330

Baba T, Ara T, Hasegawa M, Takai Y, Okumura Y, Baba M, Datsenko KA, Tomita M, Wanner BL, Mori H (2006) Construction of *Escherichia coli* K-12 in-frame, single-gene knockout mutants: the Keio collection. *Mol Syst Biol* **2,** 2006.0008

Balbontín R, Fiorini F, Figueroa-Bossi N, Casadesús J, Bossi L (2010) Recognition of heptameric seed sequence underlies multi-target regulation by RybB small RNA in Salmonella enterica. *Mol Microbiol* **78:** 380–394

Beisel CL, Storz G (2010) Base pairing small RNAs and their roles in global regulatory networks. *FEMS Microbiol Rev* **34:** 866–882

Beisel CL, Storz G (2011) The base-pairing RNA spot 42 participates in a multioutput feedforward loop to help enact catabolite repression in *Escherichia coli*. *Mol Cell* **41:** 286–297

Belasco JG (2010) All things must pass: contrasts and commonalities in eukaryotic and bacterial mRNA decay. *Nat Rev Mol Cell Biol* **11:** 467–478

Boni IV, Isaeva DM, Musychenko ML, Tzareva NV (1991) Ribosome-messenger recognition: mRNA target sites for ribosomal protein S1. *Nucleic Acids Res* **19:** 155–162

Bouvier M, Sharma CM, Mika F, Nierhaus KH, Vogel J (2008) Small RNA binding to 5′ mRNA coding region inhibits translational initiation. *Mol Cell* **32:** 827–837

Braun M, Killmann H, Maier E, Benz R, Braun V (2002) Diffusion through channel derivatives of the *Escherichia coli* FhuA transport protein. *Eur J Biochem* **269:** 4948–4959

Buchanan SK, Lukacik P, Grizot S, Ghirlando R, Ali MM, Barnard TJ, Jakes KS, Kienker PK, Esser L (2007) Structure of colicin I receptor bound to the R-domain of colicin Ia: implications for protein import. *EMBO J* **26:** 2594–2604

Cascales E, Buchanan SK, Duché D, Kleanthous C, Lloubès R, Postle K, Riley M, Slatin S, Cavard D (2007) Colicin biology. *Microbiol Mol Biol Rev* **71:** 158–229

Datsenko KA, Wanner BL (2000) One-step inactivation of chromosomal genes in *Escherichia coli* K-12 using PCR products. *Proc Natl Acad Sci USA* **97:** 6640–6645

Deana A, Belasco JG (2005) Lost in translation: the influence of ribosomes on bacterial mRNA decay. *Genes Dev* **19:** 2526–2533

Desnoyers G, Massé E (2012) Noncanonical repression of translation initiation through small RNA recruitment of the RNA chaperone Hfq. *Genes Dev* **26:** 726–739

Desnoyers G, Morissette A, Prévost K, Massé E (2009) Small RNA-induced differential degradation of the polycistronic mRNA *iscRSUA*. *EMBO J* **28:** 1551–1561

Fröhlich KS, Vogel J (2009) Activation of gene expression by small RNA. *Curr Opin Microbiol* **12:** 674–682

Gottesman S, Storz G (2010) Bacterial small RNA regulators: versatile roles and rapidly evolving variations. *Cold Spring Harb Perspect Biol* **3,** pii.a003798

Griggs DW, Tharp BB, Konisky J (1987) Cloning and promoter identification of the iron-regulated cir gene of *Escherichia coli*. *J Bacteriol* **12:** 5343–5352

Guillier M, Gottesman S (2006) Remodelling of the *Escherichia coli* outer membrane by two small regulatory RNAs. *Mol Microbiol* **59:** 231–247

Guillier M, Gottesman S (2008) The 5′ end of two redundant sRNAs is involved in the regulation of multiple targets, including their own regulator. *Nucleic Acids Res* **36:** 6781–6794

Hajnsdorf E, Boni IV (2012) Multiple activities of RNA-binding proteins S1 and Hfq. *Biochimie* **94:** 1544–1553

Hantke K (1990) Dihydroxybenzoylserine–a siderophore for *E. coli*. *FEMS Microbiol Lett* **55:** 5–8

Holmqvist E, Reimegård J, Sterk M, Grantcharova N, Römling U, Wagner EG (2010) Two antisense RNAs target the transcriptional regulator CsgD to inhibit curli synthesis. *EMBO J* **29:** 1840–1850

Hook-Barnard IG, Brickman TJ, McIntosh MA (2007) Identification of an AU-rich translational enhancer within the *Escherichia coli* fepB leader RNA. *J Bacteriol* **189:** 4028–4037

Hussein R, Lim HN (2011) Disruption of small RNA signaling caused by competition for Hfq. *Proc Natl Acad Sci USA* **108:** 1110–1115

Jacques JF, Jang S, Prévost K, Desnoyers G, Desmarais M, Imlay J, Massé E (2006) RyhB small RNA modulates the free intracellular iron pool and is essential for normal growth during iron limitation in *Escherichia coli*. *Mol Microbiol* **62:** 1181–1190

Jakes KS, Finkelstein A (2010) The colicin Ia receptor, Cir, is also the translocator for colicin Ia. *Mol Microbiol* **75:** 567–578

Kerr B, Riley MA, Feldman MW, Bohannan BJ (2002) Local dispersal promotes biodiversity in a real-life game of rock-paper-scissors. *Nature* **418:** 171–174

Kido M, Yamanaka K, Mitani T, Niki H, Ogura T, Hiraga S (1996) RNase E polypeptides lacking a carboxyl-terminal half suppress a mukB mutation in *Escherichia coli*. *J Bacteriol* **178:** 3917–3925

Kirkup BC, Riley MA (2004) Antibiotic-mediated antagonism leads to a bacterial game of rock-paper-scissors *in vivo*. *Nature* **428:** 412–414

Kleanthous C (2010) Swimming against the tide: progress and challenges in our understanding of colicin translocation. *Nat Rev Microbiol* **8:** 843–848

Komarova AV, Tchufistova LS, Supina EV, Boni IV (2002) Protein S1 counteracts the inhibitory effect of the extended Shine-Dalgarno sequence on translation. *RNA* **8:** 1137–1147

Lazdunski CJ, Bouveret E, Rigal A, Journet L, Lloubès R, Bénédetti H (1998) Colicin import into *Escherichia coli* cells. *J Bacteriol* **180:** 4993–5002

Lorenz C, Gesell T, Zimmermann B, Schoeberl U, Bilusic I, Rajkowitsch L, Waldsich C, von Haeseler A, Schroeder R (2010) Genomic SELEX for Hfq-binding RNAs identifies genomic aptamers predominantly in antisense transcripts. *Nucleic Acids Res* **38:** 3794–3808

Mangan S, Alon U (2003) Structure and function of the feed-forward loop network motif. *Proc Natl Acad Sci USA* **100:** 11980–11985

Massé E, Gottesman S (2002) A small RNA regulates the expression of genes involved in iron metabolism in *Escherichia coli*. *Proc Natl Acad Sci USA* **99:** 4620–4625

Massé E, Escorcia FE, Gottesman S (2003) Coupled degradation of a small regulatory RNA and its mRNA targets in *Escherichia coli*. *Genes Dev* **17:** 2374–2383

Massé E, Vanderpool CK, Gottesman S (2005) Effect of RyhB small RNA on global iron use in *Escherichia coli*. *J Bacteriol* **187:** 6962–6971

McCullen CA, Benhammou JN, Majdalani N, Gottesman S (2010) Mechanism of positive regulation by DsrA and RprA small

noncoding RNAs: pairing increases translation and protects rpoS mRNA from degradation. *J Bacteriol* **192:** 5559–5571

McDowall KJ, Hernandez RG, Lin-Chao S, Cohen SN (1993) The ams-1 and rne-3071 temperature-sensitive mutations in the ams gene are in close proximity to each other and cause substitutions within a domain that resembles a product of the *Escherichia coli* mre locus. *J Bacteriol* **175:** 4245–4249

Morona R, Reeves P (1982) The tolC locus of *Escherichia coli* affects the expression of three major outer membrane proteins. *J Bacteriol* **150:** 1016–1023

Moon K, Gottesman S (2011) Competition among Hfq-binding small RNAs in *Escherichia coli*. *Mol Microbiol* **82:** 1545–1562

Otaka H, Ishikawa H, Morita T, Aiba H (2011) PolyU tail of rho-independent terminator of bacterial small RNAs is essential for Hfq action. *Proc Natl Acad Sci USA* **108:** 13059–13064

Powell BS, Rivas MP, Court DL, Nakamura Y, Turnbough Jr CL (1994) Rapid confirmation of single copy lambda prophage integration by PCR. *Nucleic Acids Res* **22:** 5765–5766

Prévost K, Salvail H, Desnoyers G, Jacques JF, Phaneuf E, Massé E (2007) The small RNA RyhB activates the translation of shiA mRNA encoding a permease of shikimate, a compound involved in siderophore synthesis. *Mol Microbiol* **64:** 1260–1273

Regulski EE, Breaker RR (2008) In-line probing analysis of riboswitches. *Methods Mol Biol* **419:** 53–67

Repoila F, Gottesman S (2001) Signal transduction cascade for regulation of RpoS: temperature regulation of DsrA. *J Bacteriol* **183:** 4012–4023

Riley MA (1993a) Molecular mechanisms of colicin evolution. *Mol Biol Evol* **10:** 1380–1395

Riley MA (1993b) Positive selection for colicin diversity in bacteria. *Mol Biol Evol* **10:** 1048–1059

Riley MA, Wertz JE (2002) Bacteriocins: evolution, ecology, and application. *Annu Rev Microbiol* **56:** 117–137

Ringquist S, Jones T, Snyder EE, Gibson T, Boni I, Gold L (1995) High-affinity RNA ligands to *Escherichia coli* ribosomes and ribosomal protein S1: comparison of natural and unnatural binding sites. *Biochemistry* **34:** 3640–3648

Salvail H, Lanthier-Bourbonnais P, Sobota JM, Caza M, Benjamin JAM, Mendieta ME, Lépine F, Dozois CM, Imlay J, Massé E (2010) A small RNA promotes siderophore production through transcriptional and metabolic remodeling. *Proc Natl Acad Sci USA* **107:** 15223–15228

Salvail H, Massé E (2011) Regulating iron storage and metabolism with RNA: an overview of posttranscriptional controls of intracellular iron homeostasis. *Wiley Interdiscip Rev RNA* **3:** 26–36

Shimoni Y, Friedlander G, Hetzroni G, Niv G, Altuvia S, Biham O, Margalit H (2007) Regulation of gene expression by small non-coding RNAs: a quantitative view. *Mol Syst Biol* **3:** 138

Sledjeski DD, Gupta A, Gottesman S (1996) The small RNA, DsrA, is essential for the low temperature expression of RpoS during exponential growth in *Escherichia coli*. *EMBO J* **15:** 3993–4000

Sledjeski DD, Whitman C, Zhang A (2001) Hfq is necessary for regulation by the untranslated RNA DsrA. *J Bacteriol* **183:** 1997–2005

Storz G, Vogel J, Wassarman KM (2011) Regulation by small RNAs in bacteria: expanding frontiers. *Mol Cell* **43:** 880–891

Tjaden B, Goodwin SS, Opdyke JA, Guillier M, Fu DX, Gottesman S, Storz G (2006) Target prediction for small, noncoding RNAs in bacteria. *Nucleic Acids Res* **34:** 2791–2802

Urban JH, Vogel J (2008) Two seemingly homologous noncoding RNAs act hierarchically to activate glmS mRNA translation. *PLoS Biol* **6:** e64

Vanzo NF, Li YS, Py B, Blum E, Higgins CF, Raynal LC, Krisch HM, Carpousis AJ (1998) Ribonuclease E organizes the protein interactions in the *Escherichia coli* RNA degradosome. *Genes Dev* **12:** 2770–2781

Vogel J, Luisi BF (2011) Hfq and its constellation of RNA. *Nat Rev Microbiol* **9:** 578–589

Vytvytska O, Jakobsen JS, Balcunaite G, Andersen JS, Baccarini M, von Gabain A (1998) Host factor I, Hfq, binds to *Escherichia coli* ompA mRNA in a growth rate-dependent fashion and regulates its stability. *Proc Natl Acad Sci USA* **95:** 14118–14123

Vytvytska O, Moll I, Kaberdin VR, von Gabain A, Bläsi U (2000) Hfq (HF1) stimulates ompA mRNA decay by interfering with ribosome binding. *Genes Dev* **14:** 1109–1118

Wakeman CA, Winkler WC (2009) Analysis of the RNA backbone: structural analysis of riboswitches by in-line probing and selective 2′-hydroxyl acylation and primer extension. *Methods Mol Biol* **540:** 173–191

Wassarman KM, Repoila F, Rosenow C, Storz G, Gottesman S (2001) Identification of novel small RNAs using comparative genomics and microarrays. *Genes Dev* **15:** 1637–1651

Wiener M, Freymann D, Ghosh P, Stroud RM (1997) Crystal structure of colicin Ia. *Nature* **385:** 461–464

Yu DG, Ellis HM, Lee EC, Jenkins NA, Copeland NG, Court DL (2000) An efficient recombination system for chromosome engineering in *Escherichia coli*. *Proc Natl Acad Sci USA* **97:** 5978–5983

Zhang J, Deutscher MP (1992) A uridine-rich sequence required for translation of prokaryotic mRNA. *Proc Natl Acad Sci USA* **89:** 2605–2609

